

Conformational Simulations of Aqueous Solvated α -Conotoxin GI and Its Single Disulfide Analogues Using a Polarizable Force Field Model

Nan Jiang and Jing Ma*

School of Chemistry and Chemical Engineering, Institute of Theoretical and Computational Chemistry, Key Laboratory of Mesoscopic Chemistry of MOE, Nanjing University, Nanjing, 210093, People's Republic of China

Received: April 6, 2008; Revised Manuscript Received: June 24, 2008

The solution conformation of α -conotoxin GI and its two single disulfide analogues are simulated using a polarizable force field in combination with the molecular fragmentation quantum chemical calculation. The polarizability is explicitly described by allowing the partial charges and fragment dipole moments to be variables, with values coming from the linear-scaling energy-based molecular fragmentation calculations at the B3LYP/6–31G(d) level. In comparison with the full quantum chemical calculations, the fragmentation approaches can yield precise ground-state energies, dipole moments, and static polarizabilities for peptides. The B3LYP/6–31G(d) charges and fragment-centered dipole moments are introduced in calculations of electrostatic terms in both AmberFF03 and OPLS force fields. Our test calculations on the gas-phase glucagon (PDB code: 1gcn) and solvated α -conotoxin GI (PDB code: 1not) demonstrate that the present polarization model is capable of describing the structural properties (such as the relative conformational energies, intramolecular hydrogen bonds, and disulfide bonds) with accuracy comparable to some other polarizable force fields (ABEEM/MM and OPLS-PFF) and the quantum mechanics/molecular mechanics (QM/MM) hybrid model. The employment of fragment-centered dipole moments in calculations of dipole–dipole interactions can save computational time in comparison with those polarization models using atom-centered dipole moments without much loss of accuracy. The molecular dynamics simulations using the polarizable force field demonstrate that two single disulfide GI analogues are more flexible and less structured than the native α -conotoxin GI, in agreement with NMR experiments. The polarization effect is important in simulations of the folding/unfolding process of solvated proteins.

1. Introduction

Classical molecular simulation on the basis of force field (FF) is a practical tool to explore the structural and dynamical behavior of biomolecules. In the conventional FF models, the electrostatic potential is simply expressed in a sum of pairwise Coulombic interactions between the atom-centered point charges with fixed values.^{1,2} In many cases, it is necessary to include polarization effects explicitly. A straightforward way is the employment of induced dipoles to treat the local change in charge density around an atom.³ The higher-order multipole expansion⁴ further improves the treatment of electrostatics. Some other models combine both fixed point charges/dipoles and inducible dipoles.⁵ Similar to inducible point charge models, Drude oscillator models⁶ describe electronic induction by adding massless charged particles attached to the polarizable atoms via a harmonic spring. Belonging to another category, fluctuating charge (FQ) methods^{7–14} attempt to model the polarization response to the movement of charge density from one atom (or a bond) to another one. In the FQ model, the values of the atomic charges are treated as dynamical variables, which are derived on the basis of the principle of electronegativity equalization.^{15–23} Friesner et al. further introduced site-centered inducible dipoles into the electrostatic potential,^{9c–h} and extended the application scope to small peptides,^{9c} solvated proteins,^{9g} and protein–ligand interactions.^{9h} Pater et al. embedded fluctuating charges and dipoles into CHARMM.¹¹ In

addition, a variable internal dielectric model has been employed to implicitly consider the polarization effects in proteins with charged side chain.²⁴ Efforts have also been invested into model polarization by modifying atomic charges.^{25–27}

There is another thread of polarization models, which are framed on the basis of quantum mechanical (QM) calculations.^{28–31} However, high-level QM calculations of large-sized systems with hundreds of atoms are hindered by the high computational scaling ($O(N_{\text{basis}}^\alpha)$, where $\alpha \geq 3$ and N_{basis} is the number of basis functions) of conventional ab initio QM methods. Recently, the linear-scaling fragment-based QM calculations have been successfully applied to a variety of macromolecules.^{32–44} The central idea is to divide a macromolecule (or molecule cluster) into a series of subsystems and obtain properties of the whole molecule from a combination of those of subsystems. Among them, the energy-based approaches^{39–41} can be easily implemented at various theoretical levels and applied to geometry optimization and calculations of various properties of large-sized systems. Furthermore, by introducing the background point charges on the distant parts to mimic the electrostatic and polarization effects in the calculation of each fragment,^{34f,39d,42,43,45} the fragment-based methods can give satisfactory descriptions for many properties, such as atomic charge, dipole moment, and static polarizability.

Inspired by the successful application of the linear-scaling fragment-based methods in macromolecules, we attempt to fuse the energy-based fragmentation calculation into the polarizable force field. As shown in Figure 1, the electrostatic term (U_{elec})

* E-mail: majing@nju.edu.cn, Fax: 86-25-83596131, Tel: 86-25-83597408.

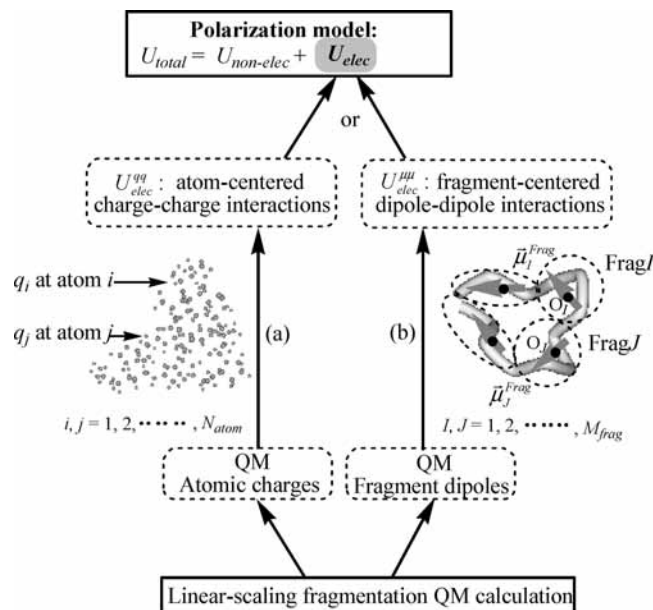


Figure 1. Schematic illustration of polarization model. The electrostatic term can be obtained from either (a) atom-centered charge–charge or (b) fragment-centered dipole–dipole interactions. O_i and O_j represent the geometric centers of the i th and j th fragments, respectively.

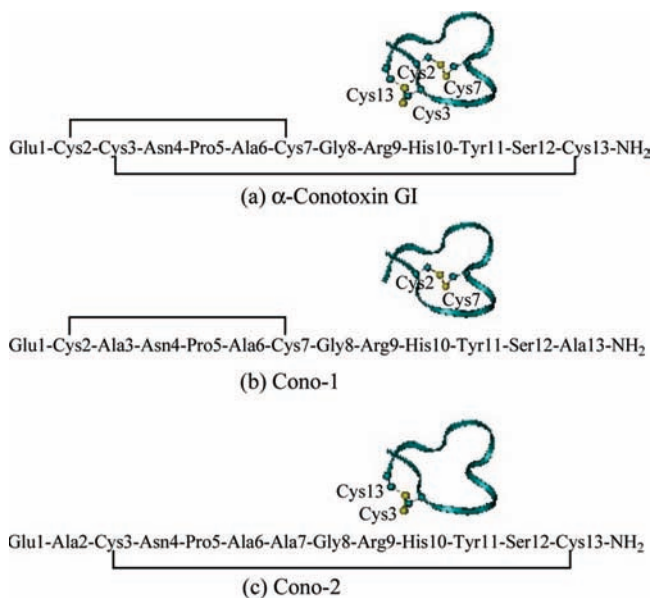


Figure 2. Amino acid sequences and cysteine frameworks for α -conotoxin GI and two models for the single disulfide analogues, Cono-1 and Cono-2. NH_2 denotes an amidated C-terminus.

of the present polarizable model differs from conventional models in two aspects: (i) The atomic partial charges are obtained directly from the linear-scaling QM calculations. This strategy is similar to the OPLS/CM1A force field,⁴⁶ which incorporates partial atomic charges obtained from semiempirical AM1 calculations. Recently, Truhlar et al. also embedded the polarizable partial charges at different levels^{47–49} in the self-consistent reaction field model for various solutions. (ii) The fragment-centered dipoles are employed in the description of polarization (Figure 1). Palmo and Krimm have mentioned that the polarization is a group property and the reduction of the number of polarizable sites is an efficient way for treating polarization.⁵⁰ It has already been demonstrated that the representation of peptide groups by dipolar structural units can give rapid evaluation of electrostatic interactions.⁵¹ In the present

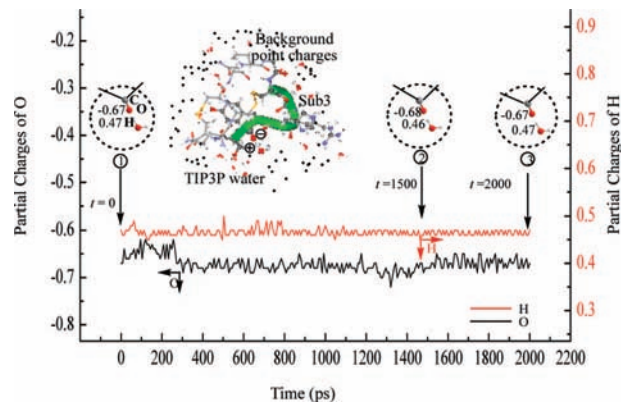


Figure 3. The variation in partial charges with the simulation time (taking the carboxyl O atom of Tyr 11 and H atom of solvent water as examples). The charges and fragment dipoles are updated case by case by using the fragmentation-based quantum mechanical calculations.


work, the introduction of fragment dipole moments in the calculation of dipole–dipole interactions (U_{elec}) does save much computational time in comparison with those using the atom-centered partial charges. The present polarizable FF can be easily implemented in the frameworks of Amber 2003 united-atom force field (FF03)^{1c} and optimized potential for liquid simulations (OPLS).² The performance of the present polarizable FF is assessed by the molecular dynamics (MD) simulations of glucagon (PDB⁵² code: 1gcn) in gas phase and solvated α -conotoxin GI (PDB⁵² code: 1not). We also make comparison of our results with the QM/MM methods and other polarizable force fields: OPLS-PFF^{9c} and OPLS-based ABEEM/MM.¹² Then, we use the present polarization model to investigate the conformational diversity and unfolding process of α -conotoxin GI, a valuable probe of nicotinic acetylcholine receptors ($n\text{AChRs}$) and ion channels,⁵³ and its two single-disulfide analogues, Cono-1 and Cono-2 (Figure 2). Our calculations show that the present FF can reasonably describe not only the relative energies of conformers but also the structural and

TABLE 1: Deviations of Energy (ΔE), Dipole Moment ($\Delta\mu$), and Static Polarizability ($\Delta\alpha$), and Average Deviations of NBO Charges ($\overline{\Delta q}$) Obtained from Energy-Based Methods with Respect to the Conventional Values for α -Conotoxin GI^a

	ΔE (kcal/mol)	$\overline{\Delta q}$	$\Delta\mu$ (Debye)	$\Delta\alpha$ (Bohr ³)
residue-based (A)	48.30	2.1×10^{-2}	5.6	261.32
secondary-structure-based (B)	-3.37	9.0×10^{-3}	1.2	46.26
GEBF ^b (C)	0.84	4.0×10^{-3}	0.3	16.47

^a All the calculations are carried out at B3LYP/6-31G(d) level.

^b GEBF calculations are carried out with details given in ref 39d.f. For α -conotoxin GI, the maximum subsystem contains 7 residues (with selected criteria of hydrogen-bond length of 2.9 Å and angle of 120.0°).

TABLE 2: Geometry Root-Mean-Square Deviations, RMSD (Å), from PDB Structure for Protein 1gcn, Calculated from Structural Optimization and NVT Molecular Dynamics Simulation with the Standard FF03 and Polarization Models, in Comparison with OPLS-PFF Results


	no H atoms			backbone only		
	FF03	FF03- <i>qq</i> (NBO)	OPLS-PFF ^a	FF03	FF03- <i>qq</i> (NBO)	OPLS-PFF ^a
optimization	1.67	1.52	3.77	1.10	1.16	2.00
MD simulation						
1 ps	2.89	2.01	4.21	2.62	1.74	2.33
2 ps	3.87	3.26	-	3.22	2.04	-

^a The OPLS-PFF results are taken from ref 9e.

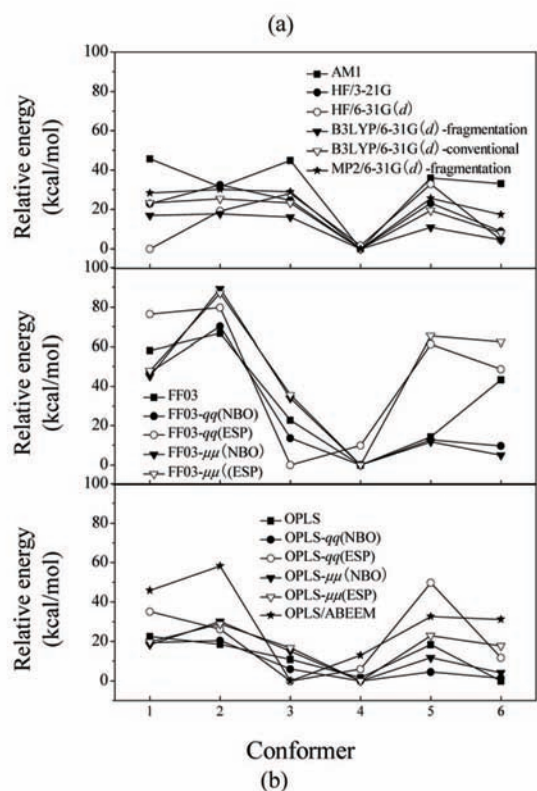
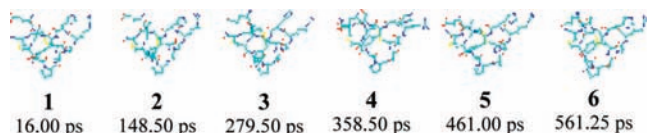


Figure 4. The (a) conformations and (b) relative energies (kcal/mol) of six α -conotoxin GI conformers, generated from MD simulations. The quantum chemical calculations are carried out at various levels including AM1, HF, conventional B3LYP, and energy-based fragmentation B3LYP and MP2 (labeled as B3LYP-fragmentation and MP2-fragmentation, respectively). The molecular mechanical calculations are implemented in conventional FF03 and OPLS force fields, respectively, with NBO or ESP charges (designated FF03(or OPLS)-*qq*(NBO) and FF03(or OPLS)-*qq*(ESP), respectively) and with fragment dipoles (designated FF03(or OPLS)- $\mu\mu$ (NBO) and FF03(or OPLS)- $\mu\mu$ (ESP), respectively).

dynamical properties of the studied systems. The molecular dynamics simulations on the conformational change of two single disulfide GI analogues reveal that the polarization effect is important in simulations of the folding/unfolding process of solvated proteins.

2. Computational Methods

2.1. Polarization Model. The present polarization model is implemented in both the FF03^{1c} and OPLS² with the potential function shown in eq 1.

$$U_{\text{total}} = U_{\text{non-elec}} + U_{\text{elec}} = \sum_{\text{bonds}} K_b(b - b_{\text{eq}})^2 + \sum_{\text{angles}} K_\theta(\theta - \theta_{\text{eq}})^2 + \sum_{\text{dihedrals}} \frac{V_n}{2}[1 + \cos(n\varphi - \gamma)] + \sum_{i < j} \left\{ \left[\frac{A_{ij}}{R_{ij}^{12}} - \frac{B_{ij}}{R_{ij}^6} \right] \right\} + U_{\text{elec}} \quad (1)$$

where all the bond stretching, angle bending, torsional rotating, and Lennard-Jones parameters are taken from the FF03^{1c} (or OPLS²) force field. The electrostatic contributions can be described by two different ways: (i) the Coulombic interactions between atomic partial charges, U_{elec}^{qq} ; and (ii) the dipole-dipole interactions between the fragment dipoles, $U_{\text{elec}}^{\mu\mu}$, as illustrated in Figure 1 and eqs 2 and 3.

$$U_{\text{elec}}^{qq} = \sum_{i < j} k \frac{q_i q_j}{R_{ij}} \quad (2)$$

$$U_{\text{elec}}^{\mu\mu} = \sum_{I < J} k \frac{1}{|\vec{R}_{IJ}|^3} \left(\vec{\mu}_I^{\text{Frag}} \cdot \vec{\mu}_J^{\text{Frag}} - 3 \frac{\vec{\mu}_I^{\text{Frag}} \cdot \vec{R}_{IJ} \cdot \vec{R}_{IJ} \cdot \vec{\mu}_J^{\text{Frag}}}{|\vec{R}_{IJ}|^2} \right) \quad (3)$$

where q_i and q_j are the atom-centered partial charges of atoms i and j , $\vec{\mu}_I^{\text{Frag}}$ and $\vec{\mu}_J^{\text{Frag}}$ are the fragment dipoles centered in fragments I and J , respectively.

As shown in Figure 3, charges and dipole moments are varied with the environment in geometry optimizations and molecular dynamics (MD) simulations. Rather than solving charges through EEM¹⁵⁻²³ and Lagrangian technique,⁵⁴⁻⁵⁷ we obtain the variable charges and fragment dipoles from the linear-scaling fragmentation QM calculations, as described in the following subsection. In this work, we use three types of FF models: (i) the standard FF03 (or OPLS) with the predetermined partial charges; (ii) FF03 (or OPLS) with the dynamically variable NBO and ESP charges taken from the linear-scaling DFT (B3LYP) calculations, designated FF03-*qq*(NBO) and FF03-*qq*(ESP), respectively; and (iii) FF03 (or OPLS) combined with the fragment dipoles calculated from NBO and ESP charges, designated FF03- $\mu\mu$ (NBO) and FF03- $\mu\mu$ (ESP), respectively. We adopted a scaling of 0.1 for the van der Waals interactions, as suggested by others.³⁰

2.2. Energy-Based Fragmentation QM Calculations. A macromolecule (or molecule cluster) is decomposed into M

TABLE 3: Relative Conformational Energies (kcal/mol) for Six α -Conotoxin GI Conformers,^a Obtained by the Standard FF03, Polarization Models with NBO and ESP Charges (Designated FF03- qq (NBO) and FF03- qq (ESP)), Respectively, and the Polarizable Model with Fragment Dipole Moments Determined by NBO and ESP Charges (Designated FF03- $\mu\mu$ (NBO) and FF03- $\mu\mu$ (ESP)), Respectively^b

conventional	force field			variable dipoles			quantum chemistry					
	atomic charges			ESP			HF					
	FF03	OPLS- qq (NBO) (ESP)	OPLS- qq (ESP)	FF03- $\mu\mu$ (NBO) (ESP)	OPLS- $\mu\mu$ (NBO) (ESP)	OPLS- $\mu\mu$ (ESP)	3-2IG	6-31G(d) ^d	6-31G(d,p)	B3LYP ^e	6-31G(d)	MP2 ^e
1	58.1	22.5	47.0 (75.8)	19.4 (35.0)	45.7 (47.6)	18.4 (19.7)	45.9	22.9	0.0 (0.0)	23.6 (16.9)	23.6 (16.9)	(28.3)
2	67.1	18.5	70.6 (79.9)	20.4 (26.2)	89.8 (87.4)	30.1 (28.8)	58.3	32.4	19.3 (19.9)	26.0 (17.8)	26.0 (17.8)	(30.2)
3	23.2	10.9	14.1 (0.0)	5.9 (0.0)	34.4 (35.9)	15.0 (16.7)	0.0	44.9	28.1 (28.3)	23.4 (16.0)	23.4 (16.0)	(29.0)
4	0.0	1.5	0.0 (9.5)	0.0 (5.9)	0.0 (0.0)	0.0 (0.0)	13.0	0.0	1.7 (1.4)	0.0 (0.0)	0.0 (0.0)	(0.0)
5	14.3	18.4	12.8 (60.9)	4.5 (49.8)	11.7 (65.4)	11.7 (22.9)	32.6	23.2	32.9 (33.2)	20.8 (10.9)	20.8 (10.9)	(25.6)
6	43.4	0.0	9.7 (48.3)	1.3 (11.8)	5.1 (62.4)	4.0 (17.7)	31.2	8.9	6.7 (7.3)	8.1 (4.4)	8.1 (4.4)	(17.3)

^aThe six conformers are taken from MD runs: 1 (16.00 ps), 2 (148.50 ps), 3 (279.50 ps), 4 (358.50 ps), 5 (461.00 ps), and 6 (561.25 ps). ^bSimilar polarization models are also embedded in OPLS force field. The quantum chemical calculations are carried out using AM1, HF, and B3LYP, and fragmentation-based B3LYP and MP2, respectively. ^cAtom-bond electronegativity equalization method fused into molecular mechanics (ABEEM/MM), as introduced in ref 12. ^dThe relative energies calculated at higher basis set level of 6-31G(d,p) are given in parenthesis. ^eThe relative energies calculated from energy-based fragmentation methods are given in parenthesis.

TABLE 4: Dihedral Angles of ϕ and φ (deg) of Solvated α -Conotoxin GI Calculated from the Standard FF03 and Polarizable Force Fields, as well as QM/MM Method, with the Deviations from X-ray Structure Given in Parentheses

residue	FF03			FF03- qq (AM1)			FF03- qq (NBO: B3LYP/6-31G(d))			QM/MM ^b			X-ray structure ^c
	FF03			FF03- qq (AM1)			fragmentation ^d			(B3LYP: AMBER)			
	ϕ	φ	deviation	ϕ	φ	deviation	ϕ	φ	deviation	ϕ	φ	deviation	
Glu 1	144.7 (13.5)	164.7 (6.5)		152.9 (5.3)	155.9 (2.3)		155.3 (2.9)	155.3 (2.9)		155.3 (2.9)	158.2		
Cys 2	118.1 (18.6)	92.5 (7.0)		98.3 (1.2)	105.7 (6.2)		96.1 (3.4)	96.1 (3.4)		96.1 (3.4)	99.5		
Cys 3	-115.6 (11.0)	-6.7 (2.0)		-10.8 (6.4)	-8.9 (4.2)		-10.6 (5.9)	-10.6 (5.9)		-10.6 (5.9)	-4.7		
Asn 4	-108.8 (26.1)	163.2 (15.3)		138.8 (17.9)	139.9 (8.0)		145.6 (2.1)	145.6 (2.1)		145.6 (2.1)	147.9		
Pro 5	-53.3 (1.5)	-38.7 (2.7)		-50.8 (4.0)	-35.6 (0.4)		-33.4 (2.6)	-33.4 (2.6)		-33.4 (2.6)	-36.0		
Ala 6	-62.4 (0.7)	-12.9 (0.6)		-65.5 (2.4)	-16.3 (2.8)		-63.1	-63.1		-63.1	-13.5		
Cys 7	-62.3 (1.4)	-40.1 (9.5)		-61.4 (0.5)	-33.0 (2.4)		-28.9 (1.7)	-28.9 (1.7)		-28.9 (1.7)	-30.6		
Gly 8	58.2 (3.9)	-137.4 (13.0)		56.7 (2.4)	-124.5 (0.1)		54.3	54.3		54.3	-124.4		
Arg 9	-59.6 (3.9)	-13.8 (0.4)		-62.8 (0.7)	-16.4 (2.2)		-65.9 (1.4)	-65.9 (1.4)		-65.9 (1.4)	-14.2		
His 10	-78.4 (16.1)	-6.7 (9.3)		-95.9 (1.4)	1.6 (4.2)		2.1 (0.5)	2.1 (0.5)		2.1 (0.5)	2.6		
Tyr 11	-56.2 (0.4)	139.5 (10.3)		138.8 (10.0)	137.2 (8.4)		125.7 (3.1)	125.7 (3.1)		125.7 (3.1)	128.8		
Ser 12	-171.7 (12.5)	116.9 (12.7)		-169.1 (10.2)	95.2 (9.0)		109.2 (5.0)	109.2 (5.0)		109.2 (5.0)	104.2		
Cys 13	-162.8 (22.1)	-153.7 (13.0)		-154.3 (13.6)	-147.9 (7.2)		-154.5 (4.7)	-154.5 (4.7)		-154.5 (4.7)	-140.7		
mean deviation	(10.5)	(10.8)		(4.2)	(4.2)		(3.0)	(3.0)		(4.1)			

^aThe secondary-structure-based scheme is employed in the fragmentation QM calculations. ^bIn the QM/MM calculation, the QM parts are described at B3LYP/6-31G(d) level. ^cX-ray results are taken from ref 53.

TABLE 5: Intramolecular Hydrogen Bonds (\AA) of Solvated α -Conotoxin GI Calculated from the Standard FF03 and Polarizable Force Fields, as Well as QM/MM Method, with the Deviations from X-ray Structure Given in Parentheses

Res ₁	Res ₂	FF03- $qq(\text{NBO})\text{B3LYP}/6-31\text{G}(\text{d})$				FF03- $qq(\text{AM1})$	FF03- $qq(\text{NBO})\text{B3LYP}/6-31\text{G}(\text{d})$		FF03- $\mu\mu(\text{NBO})\text{B3LYP}/6-31\text{G}(\text{d})$	QM/MM ^b (B3LYP: AMBER)	X-ray structure ^c
		FF03	fragmentation ^a	conventional	deviation		fragmentation ^a	conventional			
Asn 4 (⁶¹ N)	Glu 1	4.926 (2.209)	2.728 (0.011)	2.774 (0.057)	3.181 (0.464)	2.803 (0.086)	2.850 (0.133)	2.803 (0.086)	2.850 (0.133)	2.717	
Ser 12	Cys 2	2.962 (0.073)	2.778 (0.111)	2.808 (0.081)	3.197 (0.308)	3.136 (0.247)	2.993 (0.104)	3.136 (0.247)	2.993 (0.104)	2.889	
Cys 7	Asn 4	3.077 (0.192)	2.825 (0.060)	2.855 (0.030)	3.197 (0.312)	3.008 (0.123)	2.859 (0.026)	3.008 (0.123)	2.859 (0.026)	2.885	
Cly 8	Pro 5	3.259 (0.170)	3.256 (0.167)	3.106 (0.017)	3.405 (0.316)	3.443 (0.354)	3.200 (0.111)	3.443 (0.354)	3.200 (0.111)	3.089	
His 10	Cys 7	3.180 (0.312)	2.893 (0.025)	2.960 (0.092)	2.996 (0.128)	2.974 (0.106)	2.992 (0.124)	2.974 (0.106)	2.992 (0.124)	2.868	
Tyr 11	Gly 8	3.091 (0.168)	3.074 (0.151)	3.093 (0.170)	3.367 (0.444)	3.195 (0.272)	3.011 (0.088)	3.195 (0.272)	3.011 (0.088)	2.923	
Cys 2	Ser 12	2.801 (0.013)	2.659 (0.129)	2.741 (0.047)	2.801 (0.013)	2.819 (0.031)	2.807 (0.019)	2.819 (0.031)	2.807 (0.019)	2.788	
	mean deviation	(0.448)	(0.093)	(0.071)	(0.284)	(0.173)	(0.100)	(0.173)	(0.100)		

^aThe secondary-structure-based scheme is employed in the fragmentation QM calculations. ^bIn the QM/MM calculation, the QM parts are described at B3LYP/6-31G(d) level. ^cThe experimental crystal results come from ref 53.

fragments, called Fragi ($i = 1 - M_{\text{frag}}$), in the framework of energy-based fragmentation approaches. Accordingly, these fragments are constructed into M subsystems according to some criteria. Standard QM calculations are performed on these subsystems, from which the total ground-state energy of the target system can be approximately determined.³⁹⁻⁴¹ Recently, a generalized fractionation scheme was adopted for any chemical systems (including macromolecules and clusters), in which all two-fragment subsystems and most important three- or four-fragment interaction terms are included.^{39d,41c} By using a given distance or other kinds of threshold, the neighboring fragments are defined and merged with the central fragment to form the m th subsystem. Overlaps are then removed from the sum of subsystems. Since we attempt to apply the energy-based fragmentation method to proteins, it is very convenient to decompose proteins on the basis of their residue units or secondary structures. The present fragmentation procedure follows: (i) Divide a protein into several fragments. The important intramolecular hydrogen bonding interactions are explicitly considered in the QM treatment of each fragment. Electrostatic interactions coming from the distant atoms outside each fragment are approximated by the background point charges, as done in other works.^{34f,39d,42,43,45} (ii) The nearest neighboring residues attached to each fragment are included in the subsystem to mimic the influence of environment on the cutting bonds.

Obviously, the accuracy and efficiency of the molecular fragmentation methods depend on the method of dividing the whole system into fragments. For biosystems, there are several schemes for molecular decomposition, e.g., (i) we can choose each or some successive residues as a fragment, called the residue-based fragmentation (scheme A in Table 1), similar to the division of polymers by their repeating units.⁵⁸ (ii) The fragments can also be divided by the characteristic secondary structures, named the secondary-structure-based fragmentation, as shown in scheme B of Table 1. We take α -conotoxin GI as an example. It is a cyclic peptide containing 13 residues with the sequence of (Figure 2a). Two disulfide bonds, Cys2-Cys7



and Cys3-Cys13, make the protein folding with diverse secondary structures: random coil (Glu1-Cys2-Cys3-Asn4 and Ser12-Cys13), α -helix (Pro5-Ala6-Cys7), and β -turn (Gly8-Arg9-His10-Tyr11). According to its secondary structures, we simply decompose the α -conotoxin GI into four fragments (Table 1). (iii) A more general way was introduced in the GEBF approach,^{39d,f} in which two distance thresholds, ξ_1 and ξ_2 , are employed to consider neighboring fragments and important two-body terms, respectively (scheme C in Table 1). On the basis of these fragmentation schemes, the B3LYP/6-31G(d) calculations are carried out to calculate total energy, E , dipole moment, μ , and atomic charges of α -conotoxin GI. The deviations of the results obtained by energy-based methods from the conventional approach⁵⁹ are listed in Table 1. The residue-based fragmentation cannot guarantee the accurate description of energy and polarization, due to the loss of significant inter-residue interactions with such small subsystems. The deviations of energy (ΔE) and dipole moment ($\Delta\mu$) and the average deviation of NBO charges ($\Delta\bar{q}$) obtained from residue-based fragmentation are much larger than those from the secondary-structure-based and GEBF methods (Table 1). In addition, the

TABLE 6: Disulfide Bonds of Solvated α -Conotoxin GI Calculated with the Standard FF03 and Polarizable Force Fields, as Well as QM/MM Method, with the Deviations from X-ray Structure Given in Parentheses

geometry	FF03	FF03- <i>qq</i> (AM1)	FF03- <i>qq</i> (NBO)B3LYP/6-31G(d)		FF03- $\mu\mu$ (NBO) B3LYP/6-31G(d)	QM/MM ^b (B3LYP:AMBER)	X-ray structure ^c
			fragmentation ^a	conventional			
Bond Length of Disulfide Bridge							
S _{cys 2} -S _{cys 7}	2.027 (0.004)	2.038(0.007)	2.035(0.004)	2.034(0.003)	2.033(0.002)	2.034(0.003)	2.031
S _{cys 3} -S _{cys 13}	2.037 (0.018)	2.044(0.025)	2.035(0.016)	2.035(0.016)	2.040(0.021)	2.032(0.013)	2.019
Dihedral Angle of Disulfide Bridge							
C-S _{cys 2} -S _{cys 7} -C	-89.2 (2.6)	-90.4(1.4)	-89.7(2.1)	-90.7(1.1)	-89.6(2.2)	-93.7(1.9)	-91.8
C-S _{cys 3} -S _{cys 13} -C	93.1(4.3)	92.2(5.2)	92.5(4.9)	92.5(4.9)	91.9(5.5)	96.7(0.7)	97.4

^a The secondary-structure-based scheme is employed in the fragmentation QM calculations. ^b In the QM/MM calculation, the QM parts are described at B3LYP/6-31G(d) level. ^c The X-ray structure is taken from ref 53.

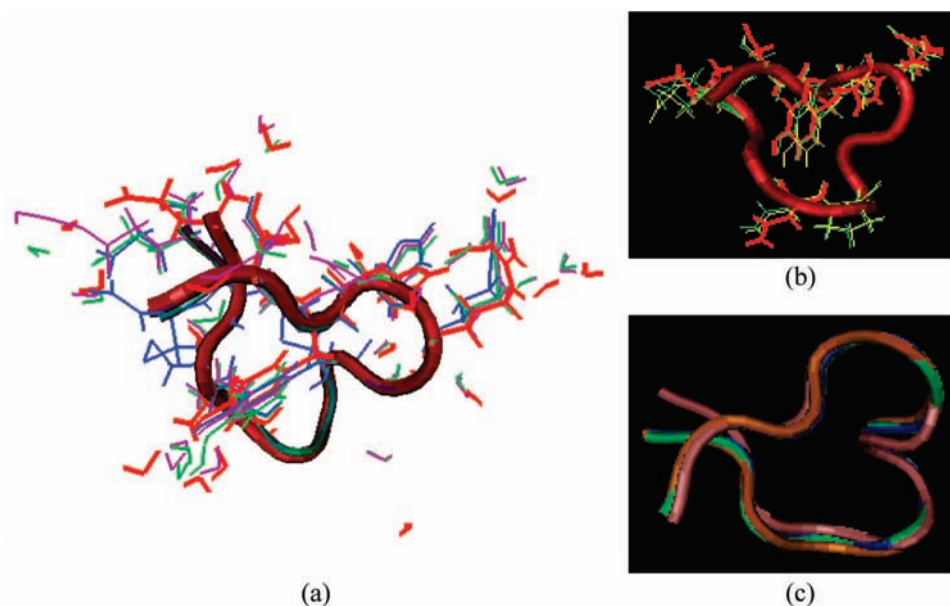


Figure 5. The optimized structures of α -conotoxin GI from FF03 (thick red tube), FF03 with fragmentation NBO charges and dipole moments (thin yellow tube), and X-ray (thin blue tube) structures. The partial charges are calculated at B3LYP/6-31G(d) level in frameworks of two fragmentations, A (residue-based: thin pink tube) and B (secondary-structure-based: thin purple tube), respectively. The polar residues are given in lines. Superposition are made with structures from (a) standard FF03, FF03 with variable charge model (fragmentation B), and experiment; (b) standard FF03, FF03 with variable charge model (fragmentation B), and FF03 with variable dipoles; (c) FF03 with NBO charges based on two fragmentations (A,B), QM/MM, and experiment.

deviations of the GEBF approach are slightly smaller than those from the secondary-structure-based fragmentation. It is not surprising, because larger subsystems are used in GEBF calculations (with the maximum size of 7 residues in each subsystem) than those (with no more than 6 residues) in the secondary-structure-based fragmentation. Since the secondary structure of a protein is very easily characterized in PDB file as well as the MD trajectory, we prefer to use this simpler secondary-structure-based fractionation in calculations of proteins.

As seen in Figure S1 of Supporting Information, the fragment-based method does take linear scaling in CPU time with the number of basis functions. The calculated atomic charges and fragment dipole moments at B3LYP/6-31G(d) level are then embedded in the force field calculations of electrostatic terms in eqs 2 and 3, with other parameters taken from FF03 or OPLS force fields. If there are large variations in conformations, our fragmentation program can automatically adjust the constituent subsystems according to the new secondary structure.

2.3. Test Calculations on the Gas-Phase Glucagon. First of all, we choose the well studied protein glucagon (PDB⁵² code: 1gcn) to test the present polarizable model. Friesner et al. has carried out an OPLS-PFF optimization and a 1 ps molecular dynamics simulation of 1gcn in gas phase,^{9e} so that we use the

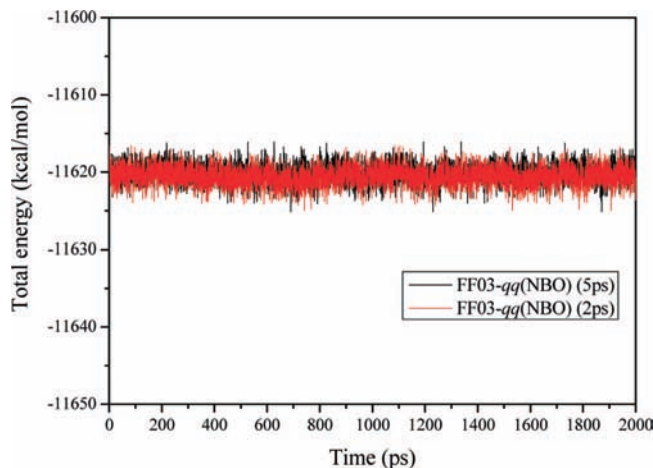


Figure 6. Energies (kcal/mol) of solvated α -conotoxin GI in MD simulations carried out in the microcanonical (constant N, V, E) ensemble. The molecular dynamics simulations are implemented in frameworks of FF03 with NBO charges, updated every 5 and 2 ps (red and black lines), respectively. The charges are obtained from energy-based fragmentation calculations at the B3LYP/6-31G(d) level.

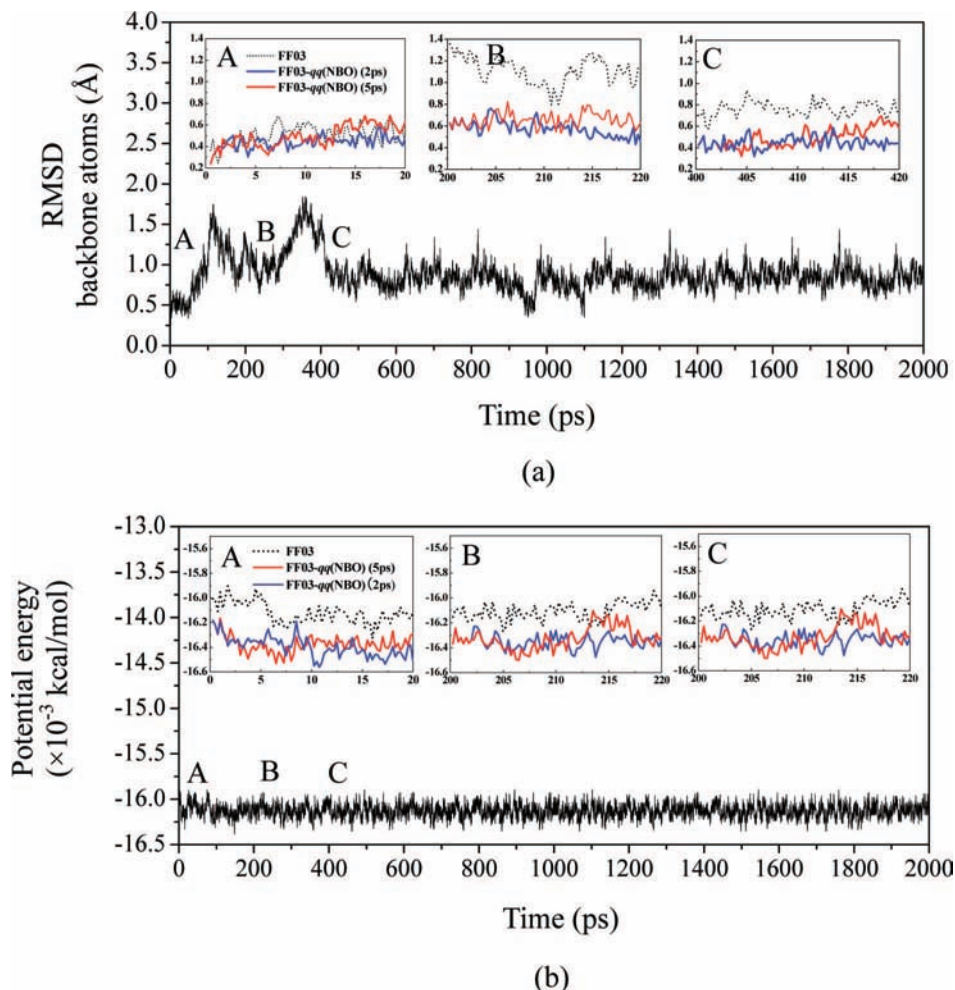


Figure 7. (a) Backbone atom root-mean-square deviations (rmsd) from the initial structure and (b) potential energies (kcal/mol) of α -conotoxin GI varied as a function of time. The molecular dynamics simulations are carried out at 300 K by using standard FF03 (dotted line) and FF03 with NBO charges, updated every 5 and 2 ps (red and blue lines), respectively. The partial charges are obtained from energy-based fragmentation calculations at the B3LYP/6-31G(d) level. Insets give amplified pictures of rmsd during A, 0–20 ps; B, 200–220 ps; and C, 400–420 ps; respectively.

same settings in calculations of both standard FF03 and our polarization models. Through cutting 1gcn (containing 471 atoms) into nine fragments (Figure S2, Supporting Information), the NBO charges are obtained from the energy-based fragmentation calculations at the B3LYP/6-31G(d) level. Then, the NBO charges are embedded in each step of energy minimization and MD simulation (at the interval of 10 fs) in the framework of the FF03-qq(NBO) model.

Table 2 shows the results of energy minimization and molecular dynamics simulation on 1gcn. The geometry root-mean-square deviations (rmsd) from the native PDB structure obtained by the fixed-charge FF03 and FF03-qq(NBO) are given. Our polarization model shows good quality, with non-H atoms rmsd of 1.52 Å and 3.26 Å for structural optimization and molecular dynamics simulation, respectively. The corresponding rmsd for backbone atoms are also very small (1.16 Å and 2.04 Å for optimization and MD, respectively). We give both 1 ps and 2 ps MD results for comparison (Table 2). The rmsd of 2 ps MD simulation are slightly larger than those of 1 ps simulation. It can be also found that the rmsd of the present polarization model have comparable accuracy to OPLS-PFF^{9c} in both energy minimization and MD simulation without the appearance of polarization catastrophe.

3. Results and Discussion

α -Conotoxin GI has been studied extensively as a prototype of venomous peptides. By replacing one pair of disulfide-bonded

Cys residues with Ala, one can obtain two analogues, Cono-1 and Cono-2, respectively (cf. Figure 2). In this section, we employ the polarization model to investigate the relative energies of α -conotoxin GI conformers, and conformational change of α -conotoxin GI and its two single disulfide analogues in aqueous solution.

3.1. Relative Energies of Conformers. The polarizable FF model is applied to calculate relative energies of different conformers of α -conotoxin GI. Six conformers are generated from MD simulations, as shown in Figure 4a. The details of MD runs will be described in subsections 3.2 and 3.3. The Cartesian coordinates of six conformers are given in Supporting Information.

QM Calculations. All the solvated water molecules are excluded in the single-point QM calculations at various levels, including AM1, HF, DFT (B3LYP), and MP2. The 3-21G, 6-31G(d), and 6-31G(d,p) basis sets are employed, respectively. The α -conotoxin GI contains 178 atoms with 1633 basis functions (at 6-31G(d) level), beyond the scope of conventional MP2 calculations. The energy-based fragmentation MP2 calculations are hence carried out instead. QM results of relative conformational energies are given in Table 3 and Figure 4b. The relative conformational energies obtained from molecular fragmentation B3LYP/6-31G(d) calculations take an order of $2 > 1 \approx 3 > 5 > 6 > 4$, consistent with that drawn from the conventional B3LYP/6-31G(d) calculations. The energy-based

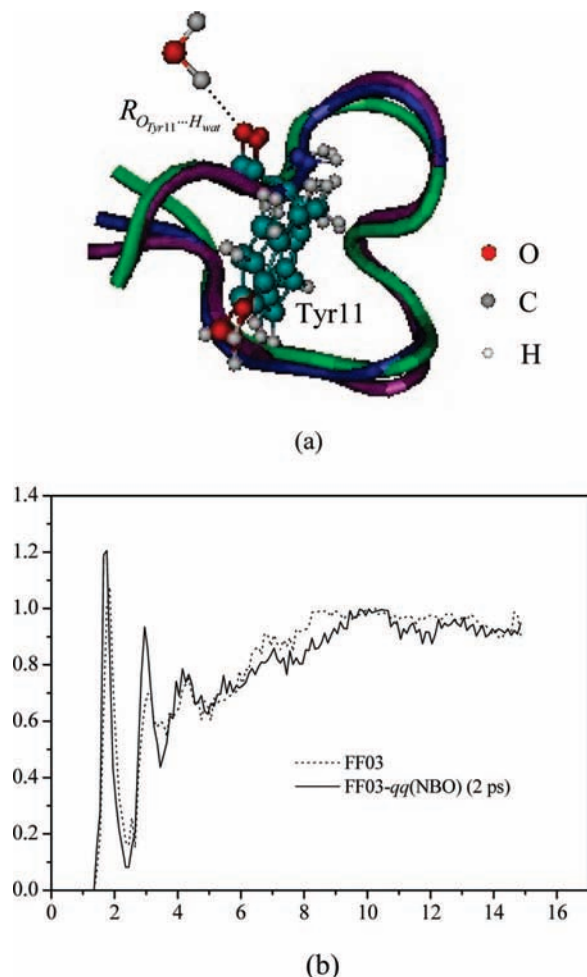


Figure 8. (a) The structure of solvated α -conotoxin GI calculated from the polarization model (purple tube), in comparison with experimental X-ray structure (blue tube) and NMR structure (green tube). (b) Radial distribution functions (RDFs) for distance between carboxyl O (of Tyr 11) and water H atoms, $R_{O_{\text{Tyr11}} \cdots H_{\text{wat}}}$. The molecular dynamics simulations are carried out by using standard FF03 (in dotted line) and the polarization model (in solid line), respectively. The fused NBO charges (at B3LYP/6–31G(d) level) in the polarizable FF03 model are updated every 2 ps.

fragmentation MP2 calculation yields a similar sequence in conformational energies to those DFT counterparts. Interestingly, conformers 1 and 3 are nearly isoenergetic but quite different in local conformations of two terminal residues, Glu 1 and Cys 13 (cf. Figure S3, Supporting Information). For each residue in these two conformers, the magnitude and direction of dipole moments also differ from each other. However, the contributions of dipole–dipole interactions between Glu 1 and Cys 13 residues are quite similar (19.3 and 19.9 kcal/mol for conformers 1 and 3, respectively, at the level B3LYP/6–31G(d)).

The HF method fails to give a correct order of conformers (at 3–21G level $2 > 3 > 5 > 1 > 6 > 4$; at 6–31G(d) and 6–31G(d,p) levels $5 > 3 > 2 > 6 > 4 > 1$), implying that the electron correlation plays an important role in proper description of this cyclic peptide. It is also apparent that the semiempirical model, AM1, cannot give good estimates for the relative energies of these conformers.

Polarization Model Implemented in FF03 and OPLS. Reproducing relative MP2 (or B3LYP) conformational energies for α -conotoxin GI is the first target of the polarization model. The relative energies obtained from the fixed-charge and several polarization models are compared in Table 3. The standard FF03

gives an incorrect order in the relative energies of the selected six conformers, in comparison with the MP2 and DFT results. In contrast, the FF03-*qq*(NBO) (FF03-based polarization model with variable NBO charges) model can rank different configurations correctly. The significant difference between FF03 and FF03-*qq*(NBO) is found for the relative energy of conformer 6. This conformer is predicted to be energetically unfavorable by FF03, in contrast to the results obtained from FF03-*qq*(NBO), B3LYP, and MP2 calculations. Although conformers 3, 5, and 6 have quite different conformations in the polar residues Glu 1 and Arg 9 (Figure S4a, Supporting Information), the partial charges within FF03 are set as the same values according to their atom types. However, the involvements of NBO charges derived from different conformational environments dramatically change the dipole moments (Figure S5, Supporting Information) and hence the electrostatic terms (Figure S4b and Table S1, Supporting Information).

To our surprise, the polarization models with NBO and ESP charges give rise to different results on α -conotoxin GI energetics. The most remarkable difference lies in the relative energies between conformers 3 and 5. This originated from the very different values (and even sometimes the sign) of partial charges raised by these two schemes in QM calculations, as exemplified by different charge distributions in terminal residue Glu 1 between conformations 3 and 5 (Figure S6, Supporting Information). The significant difference between the NBO and ESP charges has also been addressed by Yang's group.^{12a} When the fragment-centered dipole moments are applied, it can be seen from Table 3 that the relative energy order given by the FF03- $\mu\mu$ (NBO) model is consistent with those from B3LYP and MP2 calculations. However, the magnitude of relative energies is overestimated, indicating the necessity of scaling of other parameters (such as bond stretching and angle bending terms) of FF03 upon the addition of new electrostatic terms.³⁰

The present polarization model has also been implemented in the framework of the OPLS force field. The bond, angle, torsional, and Lennard-Jones parameters are retained from the OPLS-AA force field.² The electrostatic parameters are scaled by 0.5, as done in other FF methods.^{1a,2a} The relative energy orders given by OPLS-*qq*(NBO) and OPLS- $\mu\mu$ (NBO) models are also in line with those QM results.

Comparison with Other Polarization Models. A comparison is made between the present polarization model with a FQ model, atom-bond electronegativity equalization method fused into molecular mechanics (ABEEM/MM).¹² The ABEEM/MM model gives an order of $2 > 1 > 5 > 6 > 4 > 3$, which is close to the B3LYP and MP2 results. It can also be found that the performance of the present polarization FF is comparable to the ABEEM/MM.

The traditional FQ dipole models introduce $1/r^3$ dipole–dipole interactions between all atomic sites, resulting in an $O(N_{\text{atom}}^2)$ scaling, where N_{atom} is the total number of atoms (e.g., N_{atom} is 178 for α -conotoxin GI). In the present model, the fragment-centered dipole moments are involved in calculations of dipole–dipole interactions between fragments (with the total number of M_{frag} , where M_{frag} is 4 for α -conotoxin GI). The computational cost of evaluating the dipole–dipole interactions is reduced by the introduction of fragment-centered dipoles without much loss of accuracy. It is interesting to make comparison between the fragment-centered dipole moments and residue-centered dipole moments. In Table S2 (Supporting Information), the residue dipole–dipole interaction energies show larger fluctuation than the fragment ones. The explicit QM treatment of each secondary-structure-based subsystem allows

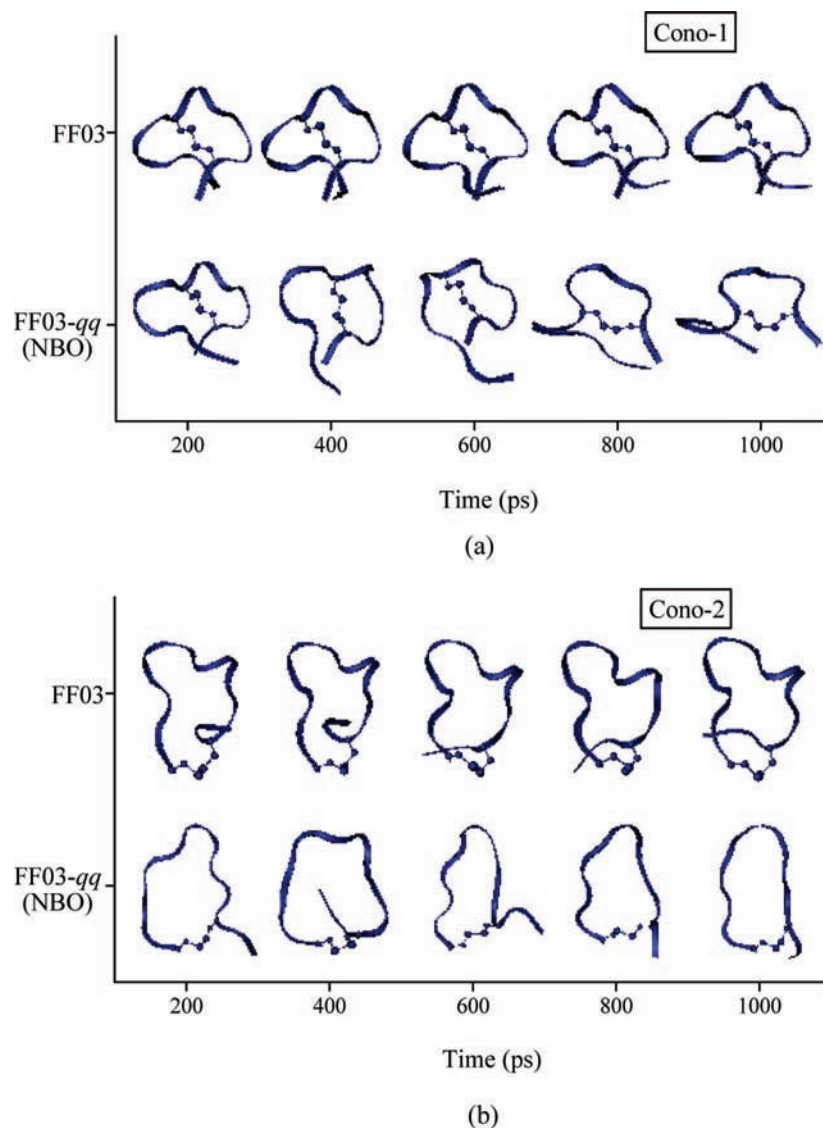


Figure 9. Snapshots of representative unfolding trajectories for (a) Cono-1 and (b) Cono-2 at several MD steps using standard FF03 (top) and polarizable FF03-*qq*(NBO) (bottom) at 300 K, respectively. In the FF03-*qq*(NBO) model, the NBO charges are calculated in the framework of molecular fragmentation method at the B3LYP/6-31G(d) level. The backbones of α -conotoxin GI analogues are shown in ribbon representations and the disulfide bonds are given in CPK forms.

the fragment-centered dipole moments to contain rich information of electrostatic interactions (such as intramolecular hydrogen bonding) in various conformational environments. In addition, the fragment dipoles can be easily extended to the coarse-grained models,⁶⁰ which have been extensively applied to macromolecules.

3.2. Structural Optimization of α -Conotoxin GI. NMR experiments⁶¹ of α -conotoxin GI in liquid water have shown small backbone rmsd of 0.95 relative to the crystal structure, indicating that the native structure does not change significantly between the liquid and the crystal. Thus, the X-ray structure of α -conotoxin GI is used as the initial geometry for energy minimizations. A supermolecular cluster (one α -conotoxin GI and 21 waters) is solvated by 1643 water molecules in a periodic rectangular box. The minimum distances from the protein atoms to the surfaces of the boxes are set to about 8.0 Å. A cutoff radius of 12.0 Å for van der Waals and electrostatic interactions is applied. The molecular mechanics minimizations are carried out with a conjugated gradient algorithm. The criterion for convergence of the variation in energy for each atom, averaged over the whole system, is set to 10^{-5} kcal/mol. The maximum number of cycles is 10 000.

The calculations are performed with both standard FF03 and our polarizable force field. The atom-centered NBO charges and fragment-centered dipole moments are adopted in simulations, respectively. In calculations with the polarization models, the partial charges and dipole moments of both the protein backbone and its vicinal 21 water molecules are allowed to fluctuate, and the other distant water molecules are represented by traditional TIP3P model, as shown in Figure 3. For the sake of comparison, the variable charges are calculated from conventional and linear-scaling fragmentation QM approaches, respectively (at B3LYP/6-31G(d) level). Results of energy minimizations for α -conotoxin GI are presented in Tables 4, 5, 6, and S3 (Supporting Information), in comparison with the QM/MM optimization results and X-ray data. In the QM/MM calculations, the α -conotoxin with 21 crystal waters forms the QM section, and some other waters form the part of MM. The DFT (B3LYP/6-31G(d)) are employed in the QM region and AMBER are used for the MM region, respectively. The QM/MM calculations are performed with Gaussian 03.⁵⁹

The conformation of the protein backbone is characterized by two torsion angles φ (C-N-C $_{\alpha}$ -C) and (N-C $_{\alpha}$ -C-N) for

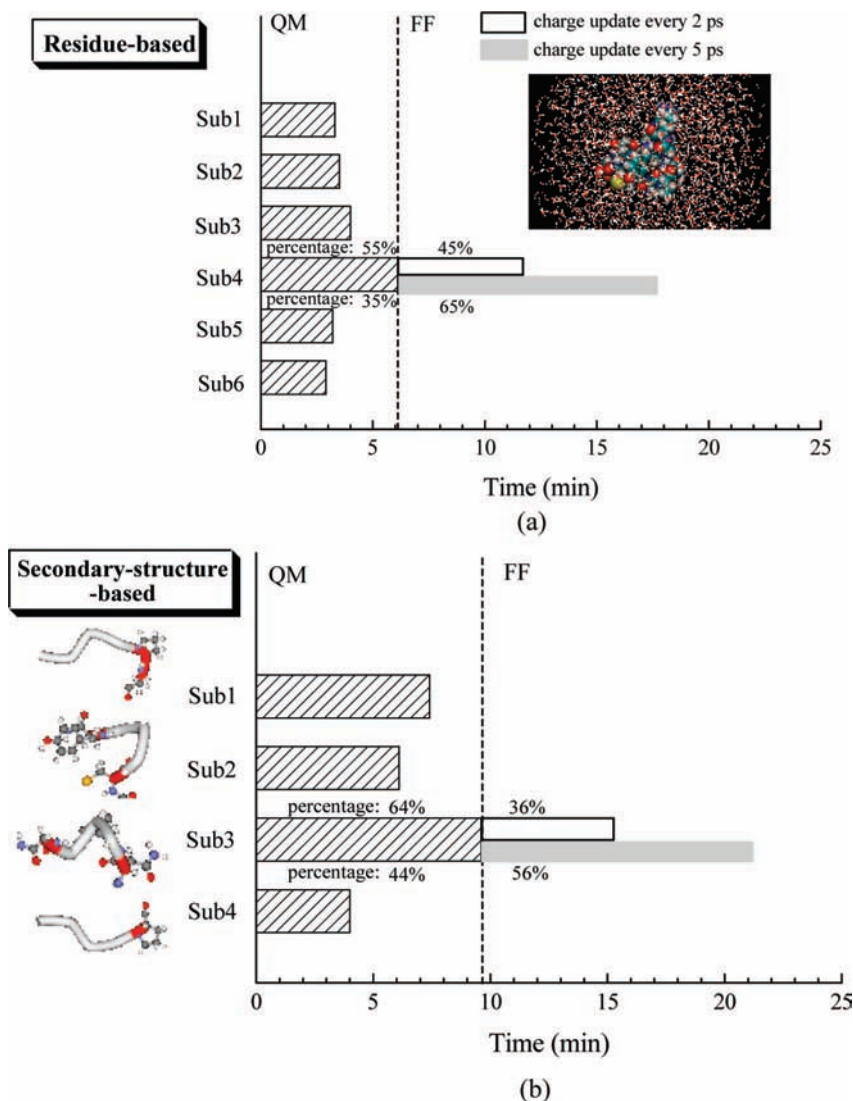


Figure 10. Computational time (in unit of minute) consumed in QM and FF parts and the corresponding percentages in the duration of one charge update step (2 and 5 ps, respectively) of molecular dynamics simulation of α -conotoxin GI using the FF03-based polarization model. Two schemes are adopted in the fragmentation-based QM calculations: (a) the residue-based and (b) the secondary-structure-based fragmentations. The time step of MD simulation is set at 0.05 fs. All the calculations are carried out on a single CPU.

each residue. As seen in Tables 4 and S3 (Supporting Information), the present polarization model at the B3LYP/6–31G(d) level performs adequately in reproducing the crystal structure. The mean deviations of ϕ and φ , from the experimental X-ray structure, obtained from the polarization models (with secondary-structure-based fragmentation B3LYP charges, 4.2° and 5.8°; with conventional B3LYP charges, 3.9° and 4.2°) are smaller than those (10.5° and 10.8°) from the standard FF03 model. The difference in the optimized backbone between the employment of fragmentation and conventional partial charges is almost negligible. In comparison to conventional calculation, the linear-scaling fragmentation approach saves CPU time to a large degree and is able to treat large-sized systems that are beyond the scope of conventional calculations.

As expected, the decrease of fragment size will harm the performance of the fragmentation-based QM calculations. As shown in Table S3 (Supporting Information), with respect to the secondary-structure-based fragmentation, the polarizable force field employing residue-based fragmentation gives larger deviations (9.7° and 7.4°) from the experiment. Thus, the inclusion of 2–3 residues in each fragment may be inadequate to describe polarization.

To further increase the efficiency of the polarization model, the fragment-centered dipoles are embedded in calculations of the electrostatic term, reducing the computational scaling from $O(N_{\text{atom}}^2)$, where $N_{\text{atom}} = 178$ for α -conotoxin GI, to $O(M_{\text{frag}}^2)$ ($M_{\text{frag}} = 4$). It can be seen from Table S3 (Supporting Information) that the replacement of atom-centered charge–charge Coulomb electrostatics by the fragment-centered dipole–dipole interactions does not affect the accuracy of the polarization model. For example, the deviations of ϕ and φ , obtained from the FF03- $\mu\mu$, are 6.1° and 6.3°, respectively, which are just slightly larger than those (4.2° and 5.8°) from the FF03- qq force fields (Table S3, Supporting Information).

It is very difficult for traditional force fields to reasonably describe the intramolecular hydrogen bonds, where polarization effects are particularly important. As displayed in Table 5, the accuracy of the polarization model (with average deviations of 0.093 Å and 0.173 Å for fragmentation FF03- qq and FF03- $\mu\mu$ force fields, respectively) from experiments is superior to that of the standard FF03 (average deviation: 0.448 Å). When conventional QM methods are applied to evaluate charges, the mean deviations of intramolecular hydrogen bonds from the X-ray structure are further reduced to 0.071 Å. The accuracy is

closely related to the proper description of hydrogen bonding interactions in each subsystem.

We also show the optimized bond lengths of disulfide bonds and the related dihedral angles in Table 6. The differences between the polarizable and nonpolarizable models are very small, indicating that disulfide bonds are relatively rigid regardless of their conformational environment.

To our encouragement, the accuracy of the present polarization model in describing the α -conotoxin GI configuration is comparable to the QM/MM model. The deviations from the experiment in torsion angles (Tables 4 and S3, Supporting Information), bond lengths of intramolecular hydrogen bonds (Table 5), and disulfide bonds (Table 6) obtained by our polarization FF model are quite close to those by the QM/MM (B3LYP: AMBER) method. It should be noticed that Gordon et al. recently gave the analytic gradients of the polarization energies in an effective fragment potential method, which is an economical method for modeling intermolecular interactions in QM/MM studies.⁶²

Finally, the optimized structures from the standard FF03 and polarization models are shown in Figure 5, in comparison with X-ray crystal structure and QM/MM result. The FF03 geometries of polar residues depart from the experimental structure to a larger degree than FF03 with variable NBO charges and fragment dipoles. Again, the secondary-structure-based fragmentation shows better performance than the residue-based method in describing the global conformations.

3.3. Conformational Simulations of α -Conotoxin GI and Its Analogues.

Computational Details. Molecular dynamics simulations are run in the canonical (constant N, V, T) ensemble at 300 K, using an extended Langevin temperature control. The simulation is carried out on the solvated α -conotoxin GI and its two analogues (Cono-1 and Cono-2) in a box with periodic boundary condition (which is the same as what used in energy minimization, subsection 3.2). The time step is set at 0.5 fs. For the native α -conotoxin GI with a compact structure cross-linked by two disulfide bonds, 8 ns MD simulation is carried out on the basis of the standard FF03 model. The time-averaged conformations, taken during periods of 1, 2, 3, 4, and 8 ns, respectively, look quite similar to each other, as shown in Figure S7 (Supporting Information). The performance of our polarization model (during the 2 ns MD run) is then compared with experiments^{53,61} and the standard FF03 method, respectively. In order to investigate the impact of the frequency of charge update on the molecular dynamics simulations, the B3LYP/6-31G(d) charges are updated every 2 and 5 ps, respectively, in different MD runs.

Periodically refreshing the QM charges suffers from the dependence of the system energy on the time elapsed since the last update. We can depress such an energetic drift by using the self-consistent NBO charges. The convergence criterion for the iterative QM calculation is set as the negligible change in total energies between two successive charge-update steps, i.e.

$$\frac{|E_{\text{total}}^{i+1} - E_{\text{total}}^i|}{E_{\text{total}}^i} \times 100\% \leq 0.02\%$$

. For the α -conotoxin GI, we find that only one iteration is good enough to obtain nearly constant total energies in MD simulation (Table S4, Supporting Information). In order to test the conservation of total energy, the 2 ns MD simulations were performed in the microcanonical (constant N, V, E) ensemble with the charges updated every 2 and 5 ps, respectively. The total energy is plotted in Figure 6 as a function of simulation

time, from which one can see that the energy does not drift much in the NVE simulations with the iterative scheme.

Conformation of Solvated α -Conotoxin GI. Figure 7a shows the backbone rmsd relative to the experimental crystal structure during 2 ns NVT simulations. The polarization models have smaller values of rmsd than the standard FF03. As expected, the FF03-based polarization model with charges updated in a shorter time interval gives smaller rmsd values than those using longer charge-update intervals. The potential energies of α -conotoxin GI, varied as a function of time in MD simulations using both classical FF03 and FF03-based polarization models, are given in Figure 7b. It can be seen that the choice of the time step for updating charge has little influence on the potential energy fluctuation.

The simulated structure of water-solvated α -conotoxin GI from the FF03-based polarization model is compared with the X-ray crystal and NMR structures in Figure 8a. One can see that the present polarization model can reproduce the experimental structures well, except in the terminal residue of Glu 1. The backbone atom rmsd from the initial structure for the N-terminal Glu 1 residue shows relatively large fluctuation (Figure S8, Supporting Information). The apparent difference in local conformations of terminal residues between the crystal (or NMR) structure and simulation has also been found in the water-solvated BPTI^{9g} and α -conotoxin MI.⁶³ The terminal residues usually bear both negative and positive charge centers (e.g., COO^- and NH_3^+ in Glu 1 of α -conotoxin GI), giving rise to significant hydrogen bonding (or more generally speaking, electrostatic interactions) between the end residues and solvent water. The water molecules move much faster relative to the backbone atoms; hence, the terminal residues change their local conformations accordingly from time to time. Therefore, local structures of the protein terminals are very sensitive to the solvent environment, making the characterization of their solution conformations a big challenge in both experiments and simulations.

Figure 8b displays the solute–solvent radial distribution functions (RDF), illustrated by distributions of the distance between the carboxyl O (of residue Tyr11) and water H atoms, labeled $R_{\text{O}_{\text{Tyr11}} \cdots \text{H}_{\text{wat}}}$. Both the standard and polarizable FF03 RDFs exhibit the first peak around 1.8 Å, indicating that a typical hydrogen bonding interaction exists between the Tyr 11 residue and water molecules. As shown in Figure 8, the polarization model predicts a slightly shorter $\text{O}_{\text{Tyr}} \cdots \text{H}_{\text{wat}}$ distance than the standard FF03 model.

Conformational Dynamics of Single Disulfide GI Analogues. It is interesting to test the performance of the present polarization model in describing the conformational dynamics of flexible proteins, such as the single disulfide analogues of α -conotoxin GI, Cono-1, and Cono-2 (Figure 2). The NMR experiment has shown that both Cono-1 and Cono-2 are considerably less structured than the native α -conotoxin GI.⁶⁴ In order to rationalize this phenomenon, MD simulations in the frameworks of both FF03 and FF03-*qq*(NBO) force fields are carried out for these two analogues, and the representative snapshots during MD runs are shown in Figure 9. It is clear that the conformational change is more evident in the framework of the polarization model than the FF03 force field. Although the FF03 shows little change in the conformations of disulfide-deleted analogues, Cono-1 and Cono-2, at 300 K, the MD simulations at 350 K do yield evident unfolding, as shown in Figure S9 (Supporting Information). The molecular dynamics simulations using the polarizable force field indicate that both Cono-1 and Cono-2 unfold gradually in the absence of a

disulfide bond, in good agreement with experiments.⁶⁴ It suggests that the formation of the second disulfide bond is indispensable to compact the backbone of peptide into the native folding.

3.4. Computational Considerations. The computational cost of the present polarization model during the MD simulation of α -conotoxin is shown in Figure 10. All the calculations are carried out on 3.0 GHz Pentium 4 workstations. Although the employment of residue-based fragmentation can save much computational time, the accuracy of this fragmentation is not satisfactory (cf. subsections 2.2 and 3.2). So, we prefer to use the secondary-structure-based fragmentation for obtaining the partial charges in the simulations of biological molecules. The most time-consuming step in the present polarization model is the QM calculation on each subsystem (usually 5–6 residues), although the fragmentation method can achieve linear scaling with the system size. Fortunately, the QM calculation of each subsystem can be carried out simultaneously on individual nodes, and highly parallel computations are accessible for the present polarization model. So, the total CPU time spending on calculations of QM charges is determined by the computational cost of the largest subsystem (for example, the third fragment of α -conotoxin GI, Figure 10b). The polarizable force field with charge updated every 2 ps (in the framework of fragmentation B3LYP/6–31G(d) calculation) increases the overall CPU time by about a factor of 2 over traditional fixed-charge force field. When the QM charges are refreshed at longer intervals (like 5 ps), the percentage of time consumption in linear-scaling fragmentation QM calculation is decreased by about 20%.

For the selected model of α -conotoxin GI with 1655 water molecules, it takes about 0.0834 and 0.0800 s to calculate electrostatic interactions by using QM/MM and FF03-*qq* methods, respectively. When fragment-based dipoles are introduced, the CPU time decreases to 0.0440 s. Furthermore, the performance of the present method is comparable to that of the QM/MM method (Tables 4–6), but it is faster than the conventional QM/MM method and it can be applied to much larger systems that are beyond the scope of the QM/MM calculations.

4. Conclusions

We have implemented a polarizable force field on the basis of the linear-scaling molecular fragmentation approach, and tested the performance of this force field in energy minimizations and molecular dynamics simulations of gas-phase glucagon and water-solvated α -conotoxin GI as well as its two single disulfide analogues. In this work, we decompose the protein molecule into several fragments according to its secondary structures, and then saturate each fragment with its nearest-neighboring residues. The background point charges are included in the calculation of each subsystem to approximately represent the long-range electrostatic interactions and polarization effects from distant parts, as done in other works.^{37f,42,46,48} On the basis of energy-based fragmentation B3LYP/6–31G(d) calculations, the QM partial charges and fragment dipoles are applied to the polarizable force field.

The present polarization model has two features. First, the partial charges and dipole moments are directly obtained from the energy-based QM calculations, without the need of parametrization. Second, fragment-centered dipole moments are used to calculate the dipole–dipole interactions. The present polarizable force field can give correct energy ordering of a series of conformers of α -conotoxin GI, with the inclusion of dipole–dipole

interactions. The simulated structures of solvated α -conotoxin GI from the polarization models are in good agreement with the experimental crystal structures. The molecular dynamics simulations using the polarization model show the less-structured conformation and unfolding process of single disulfide analogues of α -conotoxin GI, Cono-1, and Cono-2, consistent with the NMR experiment.

It has been demonstrated that the performance of the present polarization model is comparable to other polarizable force fields, such as OPLS-PFF and OPLS-based ABEM/MM as well as the QM/MM (B3LYP: AMBER) method. With the efficient fragmentation approaches, the partial charges and dipole moments can be satisfactorily calculated for any large-sized systems. The introduction of fragment-based dipole–dipole interactions in calculations of electrostatic interactions can save much computational time in comparison with those using the atom-centered charge–charge interactions. The basic idea of the fragment-based parametrization may be also applicable to reducing the complexity in treating various biological systems.

Acknowledgment. This work was supported by the National Natural Science Foundation of China (Grant No. 20433020 and 20573050), ministry of education (NCET-05–0442), and the National Basic Research Program (Grant No. 2004CB719901). We sincerely thank Prof. Zhong-Zhi Yang for providing us the ABEM/MM results on α -conotoxin GI and for helpful discussions. We greatly appreciate the good suggestions of Prof. Zhengwu Qi and Prof. Chunguang Wang (Shanghai Institute of Biochemistry and Cell Biology, Chinese Academy Science) and the reviewers.

Supporting Information Available: Cartesian coordinates of six α -conotoxin GI conformers; comparison of CPU time made between conventional method and molecular fragmentation scheme at B3LYP/6–31G(d) level (Figure S1); fragmentation scheme on the basis of secondary structure of glucagon (Figure S2); the dipole moments and their interaction energies of two residues, Glu 1 and Cys 13, in conformers 1 and 3 (Figure S3); comparisons of charges on Glu 1 of conformer 6 made between FF03 and FF03-*qq* (NBO) force fields (Figure S4); dipole moments for six conformers of α -conotoxin GI calculated by QM and MM methods (Figure S5); comparisons of NBO and ESP charges on the terminal residue Glu 1 made between conformers 3 and 5 (Figure S6); the time-averaged conformations of solvated α -conotoxin GI with standard FF03, taken from 8 ns MD simulation, in comparison with X-ray and NMR structures (Figure S7); backbone atom rmsd of Glu 1 from the initial structure of α -conotoxin GI varied as a function of time (Figure S8); snapshots of representative unfolding trajectories for Cono-1 and Cono-2 at several MD steps using standard FF03 at 300 and 350 K, respectively (Figure S9); terms of total energies for six α -conotoxin GI conformers obtained from nonpolarizable and polarizable force fields (Table S1); the dipole–dipole interaction energies of six α -conotoxin GI conformers evaluated on the basis of fragment-centered and residue-centered dipoles (Table S2); dihedral angles of solvated α -conotoxin GI calculated from the FF03-*qq*(NBO) and FF03- $\mu\mu$ (NBO) force fields (Table S3); total energy of α -conotoxin GI in different charge iteration steps during molecular dynamics simulation (Table S4). This material is available free of charge via the Internet at <http://pubs.acs.org>.

References and Notes

- (1) (a) Weiner, S. J.; Kollman, P. A.; Case, D. A.; Singh, U. C.; Ghio, C.; Alagona, G.; Profeta, S., Jr.; Weiner, P. *J. Am. Chem. Soc.* **1984**, *106*,

765. (b) Weiner, S. J.; Kollman, P. A.; Nguyen, D. T.; Case, D. A. *J. Comput. Chem.* **1986**, *7*, 230. (c) Momany, F. A.; Rone, R. *J. Comput. Chem.* **1992**, *13*, 888. (d) Cornell, W. D.; Cieplak, P.; Bayly, C. I.; Gould, I. R.; Merz, K. M.; Ferguson, D. M.; Spellmeyer, D. C.; Fox, T.; Caldwell, J. W.; Kollman, P. A. *J. Am. Chem. Soc.* **1995**, *117*, 5179. (e) Duan, Y.; Wu, C.; Chowdhury, S.; Lee, M. C.; Xiong, G.; Zhang, W.; Yang, R.; Cieplak, P.; Luo, R.; Lee, T.; Caldwell, J.; Wang, J.; Kollman, P. *J. Comput. Chem.* **2003**, *24*, 1999.
- (2) (a) Jorgensen, W. L.; Tirado-Rives, J. *J. Am. Chem. Soc.* **1988**, *110*, 1657. (b) Jorgensen, W. L.; Maxwell, D. S.; Tirado-Rives, J. *J. Am. Chem. Soc.* **1996**, *118*, 11225. (c) McDonald, N. A.; Jorgensen, W. L. *J. Phys. Chem. B* **1998**, *102*, 8049. (d) Jorgensen, W. L.; McDonald, N. A. *J. Mol. Struct. (THEOCHEM)* **1998**, *424*, 145. (e) Price, M. L. P.; Ostrovsky, D.; Jorgensen, W. L. *J. Comput. Chem.* **2001**, *22*, 1340. (f) Kaminski, G. A.; Friesner, R. A. *J. Phys. Chem. B* **2001**, *105*, 6474.
- (3) (a) There are numerical works on dipole polarizable models, e.g., Stillinger, F. H.; David, C. W. *J. Chem. Phys.* **1978**, *69*, 1473. (b) Lybrand, T. P.; Kollman, P. A. *J. Chem. Phys.* **1985**, *83*, 2923. (c) Rullmann, J. A. C.; van Duijnen, P. Th. *Mol. Phys.* **1988**, *63*, 451. (d) Sprik, M.; Klein, M. L. *J. Chem. Phys.* **1988**, *89*, 7556. (e) Cieplak, P.; Kollman, P.; Lybrand, T. *J. Chem. Phys.* **1990**, *92*, 6755. (f) Wallqvist, A.; Berne, B. J. *J. Phys. Chem.* **1993**, *97*, 13841. (g) Caldwell, J. W.; Kollman, P. A. *J. Phys. Chem.* **1995**, *99*, 6208. (h) Xie, W.; Pu, J.; MacKerell, A. D., Jr.; Gao, J. *J. Chem. Theory Comput.* **2007**, *3*, 1878. (i) Soteras, I.; Curutchet, C.; Bidon-Chanal, A.; Dehez, F.; Ángyán, J. G.; Orozco, M.; Chipot, C.; Luque, F. J. *J. Chem. Theory Comput.* **2007**, *3*, 1901.
- (4) (a) There are many theoretical works on multipole expansion, so the list here is far from complete. Stone, A. J. *J. Chem. Phys. Lett.* **1981**, *83*, 233. (b) Kosov, D. S.; Popelier, P. L. A. *J. Phys. Chem. A* **2000**, *104*, 7339. (c) Popelier, P. L. A.; Joubert, L.; Kosov, D. S. *J. Phys. Chem. A* **2001**, *105*, 8254. (d) Popelier, P. L. A.; Kosov, D. S. *J. Chem. Phys.* **2001**, *114*, 6539. (e) Sagui, C.; Pedersen, L. G.; Darden, T. A. *J. Chem. Phys.* **2004**, *120*, 73. (f) Stone, A. J. *J. Chem. Theory Comput.* **2005**, *1*, 1128.
- (5) (a) There are many theoretical works in this field. The list given below is far from complete. Mountain, R. D. *J. Chem. Phys.* **1995**, *103*, 3084. (b) Bernardo, D. N.; Ding, Y.; Krogh-Jespersen, K.; Levy, R. M. *J. Phys. Chem.* **1994**, *98*, 4180. (c) Ding, Y.; Bernardo, D. N.; Krogh-Jespersen, K.; Levy, R. M. *J. Phys. Chem.* **1995**, *99*, 11575. (d) Smith, D. E.; Dang, L. X. *J. Chem. Phys.* **1994**, *100*, 3757. (e) Gao, J.; Habibollahzadeh, D.; Shao, L. *J. Phys. Chem.* **1995**, *99*, 16460. (f) Cieplak, P.; Caldwell, J.; Kollman, P. *J. Comput. Chem.* **2001**, *22*, 1048. (g) Kaminski, G. A.; Friesner, R. A.; Zhou, R. *J. Comput. Chem.* **2003**, *24*, 267.
- (6) (a) There are many works in the field of Drude oscillator, e.g., Drude, P.; Mann, C. R.; Millikan, R. A. *The Theory of Optics*; Longmans, Green, and Co.: New York, 1902. (b) Hoye, J. S.; Stell, G. *J. Chem. Phys.* **1980**, *73*, 461. (c) Cao, J.; Berne, B. J. *J. Chem. Phys.* **1993**, *99*, 6998. (d) Lado, F. *J. Chem. Phys.* **1997**, *106*, 4707. (e) Lamoureux, G.; Roux, B. *J. Chem. Phys.* **2003**, *119*, 3025. (f) Archontis, G.; Leontidis, E.; Andreou, G. *J. Phys. Chem. B* **2005**, *109*, 17957. (g) Vorobyov, I. V.; Anisimov, V. M.; MacKerell, A. D. *J. Phys. Chem. B* **2005**, *109*, 18988. (h) Harder, E.; Anisimov, V. M.; Vorobyov, I. V.; Lopes, P. E. M.; Noskov, S. Y.; MacKerell, A. D., Jr.; Roux, B. *J. Chem. Theory Comput.* **2006**, *2*, 1587. (i) Lamoureux, G.; Harder, E.; Vorobyov, I. V.; Roux, B.; MacKerell, A. D. *J. Chem. Phys. Lett.* **2006**, *418*, 245. (j) Vorobyov, I. V.; Anisimov, V. M.; Greene, S.; Venable, R. M.; Moser, A.; Pastor, R. W.; MacKerell, A. D. *J. Chem. Theory Comput.* **2007**, *3*, 1120. (k) Anisimov, V. M.; Vorobyov, I. V.; Roux, B.; MacKerell, A. D. *J. Chem. Theory Comput.* **2007**, *3*, 1927. (l) Geerke, D. P.; van Gunsteren, W. F. *J. Chem. Theory Comput.* **2007**, *3*, 2128.
- (7) (a) Rick, S. W.; Stuart, S. J.; Berne, B. J. *J. Chem. Phys.* **1994**, *101*, 6141. (b) Rick, S. W.; Stuart, S. J.; Bader, J. S.; Berne, B. J. *J. Mol. Liq.* **1995**, *65* (66), 31. (c) Rick, S. W.; Berne, B. J. *J. Am. Chem. Soc.* **1996**, *118*, 672. (d) Rick, S. W.; Berne, B. J. *J. Phys. Chem. B* **1997**, *101*, 10488. (e) Rick, S. W. *J. Chem. Phys.* **2001**, *114*, 2276. (f) Olanow, L. R.; Rick, S. W. *J. Comput. Chem.* **2005**, *26*, 699.
- (8) Stuart, S. J.; Berne, B. J. *J. Phys. Chem.* **1996**, *100*, 11934.
- (9) (a) Liu, Y.-P.; Kim, K.; Berne, B. J.; Friesner, R. A.; Rick, S. W. *J. Chem. Phys.* **1998**, *108*, 4739. (b) Banks, J. L.; Kaminski, G. A.; Zhou, R.; Mainz, D. T.; Berne, B. J.; Friesner, R. A. *J. Chem. Phys.* **1999**, *110*, 741. (c) Stern, H. A.; Kaminski, G. A.; Banks, J. L.; Zhou, R.; Berne, B. J.; Friesner, R. A. *J. Phys. Chem. B* **1999**, *103*, 4730. (d) Stern, H. A.; Rittner, F.; Berne, B. J.; Friesner, R. A. *J. Chem. Phys.* **2001**, *115*, 2237. (e) Kaminski, G. A.; Stern, H. A.; Berne, B. J.; Friesner, R. A.; Cao, Y. X.; Murphy, R. B.; Zhou, R.; Halgren, T. A. *J. Comput. Chem.* **2002**, *23*, 1515. (f) Kaminski, G. A.; Stern, H. A.; Berne, B. J.; Friesner, R. A. *J. Phys. Chem. A* **2004**, *108*, 621. (g) Harder, E.; Kim, B.; Friesner, R. A.; Berne, B. J. *J. Chem. Theory Comput.* **2005**, *1*, 169. (h) Maple, J. R.; Cao, Y.; Damm, W.; Halgren, T. A.; Kaminski, G. A.; Zhang, L. Y.; Friesner, R. A. *J. Chem. Theory Comput.* **2005**, *1*, 694.
- (10) Yoshii, N.; Miura, S.; Okazaki, S. *J. Chem. Phys. Lett.* **2001**, *345*, 195.
- (11) (a) Patel, S.; Brooks, C. L., III *J. Comput. Chem.* **2004**, *25*, 1. (b) Patel, S.; MacKerell, A. D., Jr.; Brooks, C. L., III *J. Comput. Chem.* **2004**, *25*, 1504. (c) Patel, S.; Brooks, C. L., III *J. Chem. Phys.* **2005**, *123*, 164502.
- (12) (a) Wang, C. S.; Yang, Z. Z. *J. Chem. Phys.* **1999**, *110*, 6189. (b) Yang, Z. Z.; Wu, Y.; Zhao, D. X. *J. Chem. Phys.* **2004**, *120*, 2541. (c) Yang, Z. Z.; Zhang, Q. *J. Comput. Chem.* **2005**, *27*, 1. (d) Yang, Z. Z.; Qian, P. *J. Chem. Phys.* **2006**, *125*, 064311.
- (13) (a) Llanta, E.; Ando, K.; Rey, R. *J. Phys. Chem. B* **2001**, *105*, 7783. (b) Llanta, E.; Rey, R. *J. Chem. Phys. Lett.* **2001**, *340*, 173. (c) Ando, K. *J. Chem. Phys.* **2001**, *115*, 5228.
- (14) (a) Chelli, R.; Ciabatti, S.; Cardini, G.; Righini, R.; Procacci, P. *J. Chem. Phys.* **1999**, *111*, 4218. (b) Chelli, R.; Procacci, P. *J. Chem. Phys.* **2002**, *117*, 9175. (c) Chelli, R.; Righini, R.; Califano, S.; Procacci, P. *J. Mol. Liq.* **2002**, *96*, 97–87.
- (15) (a) Mortier, W. J.; van Genechten, K.; Gasteiger, J. *J. Am. Chem. Soc.* **1985**, *107*, 829. (b) Mortier, W. J.; Ghosh, S. K.; Shankar, S. *J. Am. Chem. Soc.* **1986**, *108*, 4315.
- (16) No, K. T.; Grant, J. A.; Scheraga, H. A. *J. Phys. Chem.* **1990**, *94*, 4732.
- (17) Rappé, A. K.; Goddard, W. A. *J. Phys. Chem.* **1991**, *95*, 3358.
- (18) Baekelandt, B. G.; Mortier, W. J.; Lievens, J. L.; Schoonheydt, R. A. *J. Am. Chem. Soc.* **1991**, *113*, 6730.
- (19) Cioslowski, J.; Stefanov, B. B. *J. Chem. Phys.* **1993**, *99*, 5151.
- (20) Ghosh, S. K. *Int. J. Quantum Chem.* **1994**, *49*, 239.
- (21) De Profijt, F.; Langenaeker, W.; Geerlings, P. *J. Mol. Struct. (THEOCHEM)* **1995**, *339*, 45.
- (22) York, D. M.; Yang, W. *J. Chem. Phys.* **1996**, *104*, 159.
- (23) (a) Yang, Z. Z.; Wang, C. S. *J. Phys. Chem. A* **1997**, *101*, 6315. (b) Yang, Z. Z.; Cui, B. Q. *J. Chem. Theory Comput.* **2007**, *3*, 1561.
- (24) Zhu, K.; Shirts, M. R.; Friesner, R. A. *J. Chem. Theory Comput.* **2007**, *3*, 2108.
- (25) Winn, P. J.; Ferenczy, G. G.; Reynolds, C. A. *J. Comput. Chem.* **1999**, *20*, 704.
- (26) Ferenczy, G. G.; Reynolds, C. A. *J. Phys. Chem. A* **2001**, *105*, 11470.
- (27) Curutchet, C.; Bofill, J. M.; Hernández, B.; Orozco, M.; Luque, F. J. *J. Comput. Chem.* **2003**, *24*, 1263.
- (28) Xie, W.; Gao, J. *J. Chem. Theory Comput.* **2007**, *3*, 1890.
- (29) Dehez, F.; Ángyán, J. G.; Gutiérrez, I. S.; Luque, F. J.; Schulten, K.; Chipot, C. *J. Chem. Theory Comput.* **2007**, *3*, 1914.
- (30) Nakagawa, S.; Mark, P.; Ågren, H. *J. Chem. Theory Comput.* **2007**, *3*, 1947.
- (31) Gresh, N.; Cisneros, G. A.; Darden, T. A.; Piquemal, J.-P. *J. Chem. Theory Comput.* **2007**, *3*, 1960.
- (32) (a) Yang, W. *Phys. Rev. Lett.* **1991**, *66*, 1438. (b) Yang, W. *Phys. Rev. A* **1991**, *44*, 7823. (c) Lee, C.; Yang, W. *J. Chem. Phys.* **1992**, *96*, 2408. (d) Yang, W.; Lee, T.-S. *J. Chem. Phys.* **1995**, *103*, 5674. (e) Zhao, Q.; Yang, W. *J. Chem. Phys.* **1995**, *102*, 9598. (f) Lee, T.-S.; York, D. M.; Yang, W. *J. Chem. Phys.* **1996**, *105*, 2744. (g) York, D. M.; Lee, T.-S.; Yang, W. *Phys. Rev. Lett.* **1998**, *80*, 5011.
- (33) (a) Dixon, S. L.; Merz, K. M. *J. Chem. Phys.* **1996**, *104*, 6643. (b) Dixon, S. L.; Merz, K. M. *J. Chem. Phys.* **1997**, *107*, 879. (c) Monard, G.; Bernal-Uruchurtu, M. I.; van der Vaart, A.; Merz, K. M.; Ruiz-López, M. F. *J. Phys. Chem. A* **2005**, *109*, 3425.
- (34) (a) Mezey, P. G. *J. Math. Chem.* **1995**, *18*, 141. (b) Mezey, P. G. *Adv. Quantum Chem.* **1996**, *27*, 163. (c) Mezey, P. G. *Int. J. Quantum Chem.* **1997**, *63*, 39. (d) Mezey, P. G. *Int. Rev. Phys. Chem.* **1997**, *16*, 361. (e) Exner, T. E.; Mezey, P. G. *J. Comput. Chem.* **2003**, *24*, 1980. (f) Exner, T. E.; Mezey, P. G. *J. Phys. Chem. A* **2004**, *108*, 4301.
- (35) (a) Zhang, D. W.; Zhang, J. Z. H. *J. Chem. Phys.* **2003**, *119*, 3599. (b) Chen, X. H.; Zhang, D. W.; Zhang, J. Z. H. *J. Chem. Phys.* **2004**, *120*, 839. (c) Chen, X. H.; Zhang, J. Z. H. *J. Chem. Phys.* **2004**, *120*, 11386. (d) Xiang, Y.; Zhang, D. W.; Zhang, J. Z. H. *J. Comput. Chem.* **2004**, *25*, 1431. (e) Zhang, D. W.; Xiang, Y.; Zhang, J. Z. H. *J. Phys. Chem. B* **2003**, *107*, 12039. (f) Zhang, D. W.; Chen, X. H.; Zhang, J. Z. H. *J. Comput. Chem.* **2003**, *24*, 1846. (g) Chen, X. H.; Zhang, Y.; Zhang, J. Z. H. *J. Chem. Phys.* **2005**, *122*, 184105. (h) Mei, Y.; Zhang, D. W.; Zhang, J. Z. H. *J. Phys. Chem. A* **2005**, *109*, 2. (i) Chen, X. H.; Zhang, J. Z. H. *J. Chem. Phys.* **2006**, *125*, 044903.
- (36) Gu, F. L.; Aoki, Y.; Korchowiec, J.; Imamura, A.; Kirtman, B. *J. Chem. Phys.* **2004**, *121*, 10385.
- (37) (a) Kitaura, K.; Ikeo, E.; Asada, T.; Nakano, T.; Uebayasi, M. *J. Chem. Phys. Lett.* **1999**, *313*, 701. (b) Kitaura, K.; Sugiki, S.-I.; Nakano, T.; Komeiji, Y.; Uebayasi, M. *J. Chem. Phys. Lett.* **2001**, *336*, 163. (c) Fedorov, D. G.; Kitaura, K. *J. Chem. Phys. Lett.* **2004**, *389*, 129. (d) Fedorov, D. G.; Kitaura, K. *J. Chem. Phys.* **2004**, *120*, 6832. (e) Fedorov, D. G.; Kitaura, K. *J. Chem. Phys.* **2005**, *122*, 054108. (f) Fedorov, D. G.; Kitaura, K. *J. Chem. Phys.* **2005**, *123*, 134103.
- (38) Hirata, S.; Valiev, M.; Dupuis, M.; Xantheas, S. S.; Sugiki, S.; Sekino, H. *Mol. Phys.* **2005**, *103*, 2255.
- (39) (a) Li, W.; Li, S. *J. Chem. Phys.* **2004**, *121*, 6649. (b) Li, S.; Li, W.; Fang, T. *J. Am. Chem. Soc.* **2005**, *127*, 7215. (c) Li, W.; Fang, T.; Li, S. *J. Chem. Phys.* **2006**, *124*, 154102. (d) Li, W.; Li, S.; Jiang, Y. *J. Phys.*

- Chem. A **2007**, *111*, 2193. (e) Cao, H.; Fang, T.; Li, S.; Ma, J. *Macromolecules* **2007**, *40*, 4363. (f) Li, S.; Li, W.; Fang, T.; Ma, J.; Jiang, Y. Low Scaling Quantum Chemical (LSQC) program; ver. 1.1; Nanjing University; Nanjing, 2006. (g) Li, S.; Li, W. *Annu. Rep. Prog. Chem., Sect. C: Phys. Chem.* **2008**, *104*, 256.
- (40) (a) Deev, V.; Collins, M. A. *J. Chem. Phys.* **2005**, *122*, 154102. (b) Collins, M. A.; Deev, V. A. *J. Chem. Phys.* **2006**, *125*, 104104.
- (41) (a) Gadre, S. R.; Shirsat, R. N.; Limaye, A. C. *J. Phys. Chem.* **1994**, *98*, 9165. (b) Babu, K.; Gadre, S. R. *J. Comput. Chem.* **2003**, *24*, 484. (c) Ganesh, V.; Dongare, R. K.; Balanarayan, D. P.; Gadre, S. R. *J. Chem. Phys.* **2006**, *125*, 104109.
- (42) Jiang, N.; Ma, J.; Jiang, Y. *J. Chem. Phys.* **2006**, *124*, 114112.
- (43) (a) Morita, S.; Sakai, S. *J. Comput. Chem.* **2001**, *22*, 1107. (b) Sakai, S.; Morita, S. *J. Phys. Chem. A* **2005**, *109*, 8424.
- (44) Bettens, R. P. A.; Lee, A. M. *J. Phys. Chem. A* **2006**, *110*, 8777.
- (45) (a) Dahlke, E. E.; Truhlar, D. G. *J. Chem. Theory Comput.* **2007**, *3*, 46. (b) Dahlke, E. E.; Truhlar, D. G. *J. Chem. Theory Comput.* **2008**, *4*, 1. (c) Dahlke, E. E.; Leverentz, H. R.; Truhlar, D. G. *J. Chem. Theory Comput.* **2008**, *4*, 33.
- (46) Jorgensen, W. L.; Jensen, K. P.; Alexandrova, A. N. *J. Chem. Theory Comput.* **2007**, *3*, 1987.
- (47) Marenich, A. V.; Olson, R. M.; Kelly, C. P.; Cramer, C. J.; Truhlar, D. G. *J. Chem. Theory Comput.* **2007**, *3*, 2011.
- (48) Olson, R. M.; Marenich, A. V.; Cramer, C. J.; Truhlar, D. G. *J. Chem. Theory Comput.* **2007**, *3*, 2046.
- (49) Marenich, A. V.; Olson, R. M.; Chamberlin, A. C.; Cramer, C. J.; Truhlar, D. G. *J. Chem. Theory Comput.* **2007**, *3*, 2055.
- (50) Palmo, K.; Krimm, S. *J. Chem. Theory Comput.* **2007**, *3*, 2120.
- (51) Niedermeier, C.; Tavan, P. *J. Chem. Phys.* **1994**, *101*, 734.
- (52) Berman, H. M.; Westbrook, J.; Feng, Z.; Gilliland, G.; Bhat, T. N.; Weissig, H.; Shindyalov, I. N.; Bourne, P. E. *Nucleic Acid Res.* **2000**, *28*, 235.
- (53) Guddat, L. W.; Martin, J. A.; Shan, L.; Edmundson, A. B.; Gray, W. R. *Biochemistry* **1996**, *35*, 11329.
- (54) Andersen, H. C. *J. Chem. Phys.* **1980**, *72*, 2384.
- (55) Parrinello, M.; Rahman, A. *Phys. Rev. Lett.* **1980**, *45*, 1196.
- (56) Car, R.; Parrinello, M. *Phys. Rev. Lett.* **1985**, *55*, 2471.
- (57) Nosé, S. *Mol. Phys.* **1984**, *52*, 225.
- (58) Li, H.; Li, W.; Li, S.; Ma, J. *J. Phys. Chem. B* **2008**, *112*, 7061.
- (59) Frisch, M. J.; Trucks, G. W.; Schlegel, H. B.; Scuseria, G. E.; Robb, M. A.; Cheeseman, J. R.; Montgomery, J. A.; Vreven, T.; Kudin, K. N.; Burant, J. C.; Millam, J. M.; Iyengar, S. S.; Tomasi, J.; Barone, V.; Mennucci, B.; Cossi, M.; Scalmani, G.; Rega, N.; Petersson, G. A.; Nakatsuji, H.; Hada, M.; Ehara, M.; Toyota, K.; Fukuda, R.; Hasegawa, J.; Ishida, M.; Nakajima, T.; Honda, Y.; Kitao, O.; Nakai, H.; Klene, M.; Li, X.; Knox, J. E.; Hratchian, H. P.; Cross, J. B.; Bakken, V.; Adamo, C.; Jaramillo, J.; Gomperts, R.; Stratmann, R. E.; Yazyev, O.; Austin, A. J.; Cammi, R.; Pomelli, C.; Ochterski, J. W.; Ayala, P. Y.; Morokuma, K.; Voth, G. A.; Salvador, P.; Dannenberg, J. J.; Zakrzewski, V. G.; Dapprich, S.; Daniels, A. D.; Strain, M. C.; Farkas, O.; Malick, D. K.; Rabuck, A. D.; Raghavachari, K.; Foresman, J. B.; Ortiz, J. V.; Cui, Q.; Baboul, A. G.; Clifford, S.; Cioslowski, J.; Stefanov, B. B.; Liu, G.; Liashenko, A.; Piskorz, P.; Komaromi, I.; Martin, R. L.; Fox, D. J.; Keith, T.; Al-Laham, M. A.; Peng, C. Y.; Nanayakkara, A.; Challacombe, M.; Gill, P. M. W.; Johnson, B.; Chen, W.; Wong, M. W.; Gonzalez, C.; Pople, J. A. *Gaussian 03*, revision D.01; Gaussian, Inc.: Wallingford, CT, 2004.
- (60) (a) See, for example, Succi, N. D.; Onuchic, J. N.; Wolynes, P. G. *J. Chem. Phys.* **1996**, *104*, 5860. (b) Takada, S.; Luthey-Schulten, Z.; Wolynes, P. G. *J. Chem. Phys.* **1999**, *110*, 11616. (c) Murtola, T.; Falck, E.; Patra, M.; Karttunen, M.; Vattulainen, I. *J. Chem. Phys.* **2004**, *121*, 9156. (d) Marrink, S. J.; de Vries, A. H.; Mark, A. E. *J. Phys. Chem. B* **2004**, *108*, 750. (e) Baron, R.; de Vries, A. H.; Hünenberger, P. H.; van Gunsteren, W. F. *J. Phys. Chem. B* **2006**, *110*, 8464. (f) Baron, R.; de Vries, A. H.; Hünenberger, P. H.; van Gunsteren, W. F. *J. Phys. Chem. B* **2006**, *110*, 15602. (g) Han, W.; Wu, Y.-D. *J. Chem. Theory Comput.* **2007**, *3*, 2146.
- (61) Pardi, A.; Galdes, A.; Florance, J.; Maniconte, D. *Biochemistry* **1989**, *28*, 5494.
- (62) Li, H.; Netzloff, H. M.; Gordon, M. S. *J. Chem. Phys.* **2006**, *125*, 194103.
- (63) Gouda, H.; Yamazaki, K.; Hasegawa, J.; Kobayashi, Y.; Nishiuchi, Y.; Sakakibara, S.; Hirono, S. *Biochim. Biophys. Acta* **1997**, *1343*, 327.
- (64) Kaerner, A.; Rabenstein, D. L. *Biochemistry* **1999**, *38*, 5459.